Hindawi Publishing Corporation
Journal of Electrical and Computer Engineering
Volume 2012, Article ID 218930, 9 pages
doi:10.1155/2012/218930

Research Article

Ranging Performance of the IEEE 802.15.4a UWB Standard under FCC/CEPT Regulations

Thomas Gigl,[1] Florian Troesch,[2] Josef Preishuber-Pfluegl,[3] and Klaus Witrisal[1]

[1] *Signal Processing and Speech Communication Laboratory, Graz University of Technology 8010 Graz, Austria*
[2] *Communication Technology Laboratory, Swiss Federal Institute of Technology (ETH), 8092 Zurich, Switzerland*
[3] *CISC Semiconductor, Design and Consulting GmbH, 9020 Klagenfurt, Austria*

Correspondence should be addressed to Thomas Gigl, thomas.gigl@gmail.com

Received 25 October 2011; Accepted 29 January 2012

Academic Editor: Hsien-Chin Chiu

The IEEE 802.15.4a standard for wireless sensor networks is designed for high-accuracy ranging using ultra-wideband (UWB) signals. It supports coherent and noncoherent (energy detector) receivers, thus the performance-complexity-tradeoff can be decided by the implementer. In this paper, the maximum operating range and the maximum allowed pathloss are analyzed for ranging and both receiver types, under FCC/CEPT regulations. The analysis is based on the receiver working points and a link budget calculation assuming a frees-pace pathloss model. It takes into consideration the parameters of the preamble, which influence the transmit power allowed by the regulators. The best performance is achieved with the code sequences having the longest pulse spacing. Coherent receivers can achieve a maximum operating range up to several thousand meters and energy detectors up to several hundred meters.

1. Introduction

Real-time locating systems (RTLSs) and sensor networks are challenging topics for research and development. Novel applications, such as the tracking of fire fighters in emergencies [1, 2] and the tagging of cars in the manufacturing process, need very precise and reliable localization in multipath intensive environments. Common approaches as, for example, the global positioning system (GPS) or WLAN fail in such situations, because the signals are unable to penetrate the roof and the walls and/or they get disturbed by multipath propagation. Thus, researchers have focused on new radio frequency (RF) technologies in recent years, in particular ultra-wideband (UWB). UWB shows robustness against multipath interference and allows for highly accurate positioning [3–9].

IEEE 802.15.4a [10] is a standard for wireless sensor networks with submeter ranging accuracy in indoor environments. The physical layer is designed for bidirectional communications using amplitude and position modulated, bandpass-type UWB signals. It thus supports high-complexity coherent receivers and low-complexity energy detectors. A two-way time of arrival ranging scheme is proposed. The first part of each transmission is a pulse sequence with known codes, called the preamble, which is used for signal detection, synchronization, and the estimation of the channel impulse response (CIR) that is needed to obtain the time-of-arrival. The preamble sequences show perfect autocorrelation properties for both receiver types [11]. Energy detectors promise low cost and low power consumption, but a performance loss occurs [12] and more vulnerability is unavoidable with respect to interfering signals [13]. Sub-Nyquist-rate sampling can further reduce the complexity, but also the ranging performance [7, 14].

The IEEE 802.15.4a standard has a large number of system parameters that influence the achievable ranging performance [15–17]. Based on the results in [18], the maximal allowed transmit power is analyzed in this paper taking into account the regulations of the Federal Communication Commission (FCC) [19] and the Conférence Européenne des Postes et Télécommunications (CEPT) [20]. The system performance is evaluated with respect to the achievable operating range and the maximum allowed pathloss for a coherent receiver and an energy detector. Our analysis shows the parameter settings and frequency channel selection for maximizing the performance.

Table 1: Preamble characteristic.

N_s	L	N_{pr}	T_{chip} (ns)	T_{pr} (μs)	PRF (MHz)	MRF (MHz)	ERF (MHz)	$N_{1\,\text{ms}}$
31	16	16	≈2	15.9	31.2	16.1	**0.256**	16
31	16	64	≈2	63.6	31.2	16.1	1.024	64
31	16	256	≈2	254.4	31.2	16.1	4.096	256
31	16	1024	≈2	**1017.4**	31.2	16.1	16.1	1006
31	16	4096	≈2	**4069.7**	31.2	16.1	16.1	1006
31	64	16	≈2	63.6	7.8	4.03	**0.256**	16
31	64	64	≈2	254.4	7.8	4.03	1.024	64
31	64	256	≈2	**1017.4**	7.8	4.03	4.03	251
31	64	1024	≈2	**4069.7**	7.8	4.03	4.03	251
31	64	4096	≈2	**16279.0**	7.8	4.03	4.03	251
127	4	16	≈2	16.3	124.8	62.89	1.024	16
127	4	64	≈2	65.1	124.8	62.89	4.096	64
127	4	256	≈2	260.5	124.8	62.89	16.384	256
127	4	1024	≈2	**1042.1**	124.8	62.89	62.89	982
127	4	4096	≈2	**4168.2**	124.8	62.89	62.89	982

The paper is organized as follows. Section 2 presents the signal models according to the 802.15.4a standard, a signal-to-noise ratio (SNR) analysis, and the performance metric definition. The FCC and CEPT regulations are discussed in Section 3, and the link budget is introduced in Section 4. This is followed by performance results and conclusions in Sections 5 and 6.

2. Problem Statement

An (indoor) ranging system needs to find the line-of-sight (LOS) component in the channel response, because the detection of a reflection or a noise component may lead to very large errors. Thus, the ranging performance can be characterized by the quality of the channel estimation at the receiver output. An appropriate performance metric is the receiver output SNR of the LOS component (LSNR), as it correlates strongly with the ranging performance [21]. It is defined as

$$\text{LSNR} = \frac{|y_s[n_{\text{LOS}}]|^2}{\text{var}\{\widehat{h}[n]\}}, \tag{1}$$

where $y_s[n_{\text{LOS}}]$ is the LOS sample n_{LOS} of the receiver output and $\text{var}\{\widehat{h}[n]\}$ is the noise variance of the estimated channel response $\widehat{h}[n]$.

To study the operating range, it is necessary to relate the output SNR to the input SNR of the receiver. The input SNR is given by the transmit power regulations, the link budget, and the channel. The output SNR furthermore depends on the receiver structure, the hardware components, and—in case of a noncoherent receiver—also on the preamble parameters, as analyzed below. The input SNR is defined by the energy of the despread LOS component over the noise spectral density E_{LOS}/N_0 with $E_{\text{LOS}} = M_1 E_{\text{LOS}}^{(1)}$, where $E_{\text{LOS}}^{(1)}$ is the received energy for the LOS component of a single pulse and M_1 is the number of transmitted pulses.

2.1. Signal Models. This section introduces the signal models for the IEEE 802.15.4a physical layer and the receivers.

2.1.1. IEEE 802.15.4a. The most important signal part for ranging is the preamble. It employs a code sequence $\mathbf{c}_s$ of length $N_s = 31$ or 127 [10] that consists of ternary elements $\{-1, 0, 1\}$. The preamble code vector $\mathbf{c}_{\text{sp}}$ is created as

$$\mathbf{c}_{\text{sp}} = \mathbf{1}_{N_{\text{pr}}} \otimes \mathbf{c}_s \otimes \boldsymbol{\delta}_L = \mathbf{c} \otimes \boldsymbol{\delta}_L, \tag{2}$$

where $\otimes$ denotes the Kronecker product, $\boldsymbol{\delta}_L$ is a unit vector with a one at the first position and length L to extend the spacing between the preamble chips, and $\mathbf{1}_{N_{\text{pr}}}$ denotes a vector of ones to repeat the preamble sequence N_{pr} times. The vector $\mathbf{c}$ is the periodically repeated preamble code. The transmitted signal $s(t)$ is defined as

$$\begin{aligned} s(t) &= \Re\left\{\sqrt{E_p}\sum_{m=0}^{M-1} c_m w\left(t - mLT_{\text{chip}}\right) e^{j\omega_c t}\right\} \\ &= \sqrt{E_p}\sum_{m=0}^{M-1} c_m \widetilde{w}\left(t - mLT_{\text{chip}}\right), \end{aligned} \tag{3}$$

where E_p is the energy per pulse, c_m is the m-th element of $\mathbf{c}$, $w(t)$ is the energy-normalized pulse shape, M is the number of code elements in the preamble, ω_c is the carrier frequency, T_{chip} is the chip duration, and $\widetilde{w}(t)$ is the upconverted pulse assuming the carrier and the pulse are phase synchronous.

Table 1 shows the timing characteristics of the preamble, where T_{pr} is the total duration of the preamble, PRF is the peak pulse repetition frequency, MRF is the mean pulse repetition frequency, and $N_{1\,\text{ms}}$ is the number of preamble sequences within 1 ms. ERF is the effective pulse repetition frequency according to the regulations (see Section 3).

The transmitted signal (3) is sent over a multipath channel with channel impulse response $h_c(t)$, where also the effects of the antenna are contained for simplicity.

Furthermore, $h_c(t)$ is assumed to be constant during T_{pr}. Thus, the analog received signal is obtained from

$$r_a(t) = s(t) * h_c(t) + \nu(t), \tag{4}$$

where $\nu(t)$ is modeled as additive white Gaussian noise and $*$ is the convolution. Next, the receiver architectures are described.

2.1.2. Coherent Receiver. Figure 1 shows the system model of the coherent receiver. The signal is received by a UWB antenna and filtered by the transmit pulse shape $\widetilde{w}(t)$. Thus, a matched filtering to the pulse shape is applied. The signal is converted to complex baseband using the Hilbert transform $h_{\text{hilb}}(t)$ and carrier demodulation by the estimated frequency $\hat{\omega}_c$. The complex baseband signal is given by

$$r_b(t) = [r_a(t) * \widetilde{w}(t) * h_{\text{hilb}}(t)]e^{-j\hat{w}_c t+\varphi}, \tag{5}$$

where φ is the unknown carrier phase. Assuming synchronization and known carrier frequency, an estimated sampled channel response is obtained after despreading,

$$\hat{h}[n] = M_1 h[n] + \sum_{q=0}^{N_{\text{pr}}-1}\sum_{m=0}^{N_s-1} c_m \nu_b\Big[n + (m+qN_s)LN_{\text{chip}}\Big], \tag{6}$$

because the preamble codes have perfect circular autocorrelation properties, thus interpulse interference (IPI) is canceled. (For this assumption it is necessary that the maximal excess delay $\tau_{\max} \le LN_sT_{\text{chip}} = T_s$, where T_s is the period of the spread preamble sequence. The IEEE 802.15.4a standard has a $T_s \ge 1\,\mu$s, which is usually sufficient for IPI free processing in indoor environments.) The despreading is first performed sequencewise ($\sum_m$) and then over the sequence repetitions ($\sum_q$). Since $c_m^2 = 1$ for the nonzero code elements, it follows that $\sum_q$ and $\sum_m$ simply the number of nonzero code elements in the preamble $M_1 = ((N_s{+}1)/2)N_{\text{pr}}$, that is, the number of transmitted pulses. The number of samples within a chip is defined by $N_{\text{chip}} = T_{\text{chip}}/T$. The noise $\nu_b[n]$ is the band-limited input noise $\nu_b[n] = \nu[n] * w[n]$ in complex baseband. A detailed derivation of the equations can be found in [15].

This receiver architecture needs high sampling rates according to the Nyquist theorem. Another disadvantage of this concept is the required synchronization of the carrier frequency and phase, which is critical for its performance. The energy detector is based on a different method for the downconversion that prevents these two problems. Thus, a low-complexity solution is obtained.

2.1.3. Energy Detector. The energy detector works as shown in Figure 2. The signal is again received by a UWB antenna and filtered by a bandpass filter, which ideally is matched to the pulse shape. Next, the signal is squared and integrated for short-time windows T_I. The length of T_I also defines the sampling period. It causes a mean absolute error (MAE) of ranging greater or equal $T_I/4$ [7], which limits T_I to a few ns

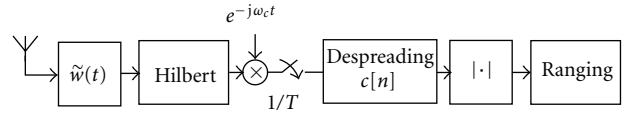

Figure 1: Coherent receiver.

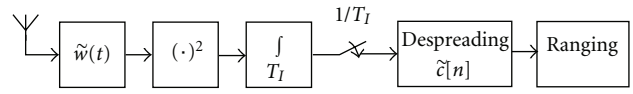

Figure 2: Energy detector.

for highly accurate ranging. The signal model after sampling is given by

$$\begin{aligned} x[n] &= \int_{nT_I}^{(n+1)T_I} (r_a(t) * \widetilde{w}(t))^2 dt \\ &= \int_{nT_I}^{(n+1)T_I} \left(\sum_{m=0}^{M-1} c_m g\Big(t - mLT_{\text{chip}}\Big) + \nu_f(t)\right)^2 dt, \end{aligned} \tag{7}$$

where $\nu_f(t)$ is the passband filtered noise and the channel response $g(t) = \sqrt{E_p}\phi_{\widetilde{w}}(t) * h_c(t + mLT_{\text{chip}})$ and $\phi_{\widetilde{w}}(t)$ is the autocorrelation function of $\widetilde{w}(t)$. The estimated channel response $y[n]$ is obtained by despreading $x[n]$,

$$\begin{aligned} y[n] &= \sum_{q=0}^{N_{\text{pr}}-1}\sum_{i=0}^{N_s-1} \widetilde{c}_i x\Big[n + i\widetilde{LN}_{\text{chip}} + qN_sL\widetilde{N}_{\text{chip}}\Big] \\ &= y_{ss}[n] + y_{s\nu}[n] + y_{\nu\nu}[n], \end{aligned} \tag{8}$$

where $\widetilde{N}_{\text{chip}} = T_{\text{chip}}/T_I$. The code despreading is performed sequencewise with $\sum_q$ and $\sum_i$ with the despreading code $\widetilde{c}_i$. In contrast to the coherent receiver, the noncoherent receiver uses a different despreading code $\widetilde{\mathbf{c}}$ than the spreading code to obtain perfect circular correlation properties for the squared sequences. This code is created by squaring $\mathbf{c}$ and setting all zeros to -1 [11]. The output of the energy detector comprises a signal-by-signal term $y_{ss}[n]$, a linear signal-by-noise term $y_{s\nu}[n]$, and a quadratic noise-by-noise term $y_{\nu\nu}[n]$. The code correlation can completely cancel the IPI in the signal term $y_{ss}[n]$ but not for the cross-term $y_{s\nu}[n]$. A longer pulse spacing leads to less IPI such that it becomes negligible in indoor environments with a spacing of $L \ge 16$ [15, 16]. The full derivation of the equations can also be found in these references.

2.2. Input-to-Output SNR Relation. The input-to-output SNR relation for the coherent receiver is given by [15]

$$\text{LSNR}_{\text{CR}} = \frac{E_{\text{LOS}}}{N_0}. \tag{9}$$

For the energy detector, the relation is given by [15, 16]

$$\text{LSNR}_{\text{ED}} = \frac{2(E_{\text{LOS}}/N_0)^2}{4(E_{\text{LOS}}/N_0) + N_sN_{\text{pr}}T_IW_{\text{RRC}}}, \tag{10}$$

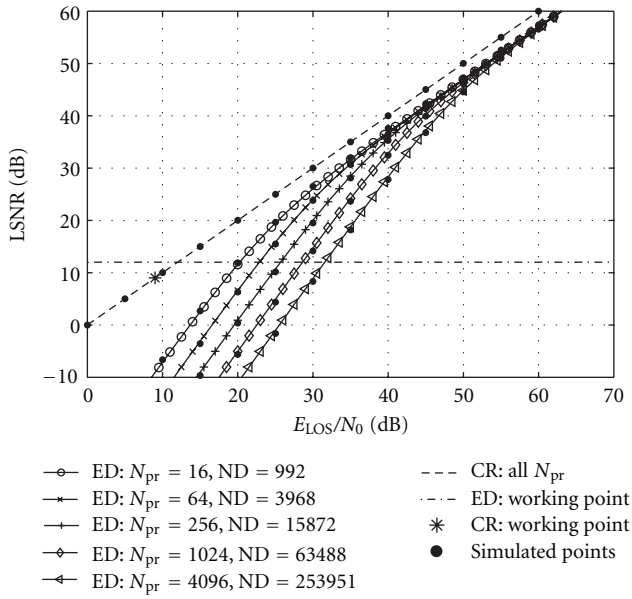

Figure 3: Relation between input SNR (E_{LOS}/N_0) and output SNR (LSNR) with respect to the noise dimensionality ND = $N_s N_{pr} T_I W_{RRC}$ for the energy detector (ED) and the coherent receiver (CR). The fixed parameters are $N_s = 31$, $T_I = 2.0032$ ns, and $W_{RRC} = 1$ GHz.

where W_{RRC} is an equivalent bandwidth defined as $W_{RRC} = \int \phi_{\tilde{w}}^2(\mu)d\mu$. The first and second terms of the denominator correspond to the variance of the linear and the quadratic noise terms, respectively. The quadratic noise term depends on the receiver parameters that can be combined to the noise dimensionality ND = $N_s N_{pr} T_I W_{RRC}$ [13]. For practical values of ND, the output SNR is proportional to $(E_{LOS}/N_0)^2$, while it shows a linear relation to E_{LOS}/N_0 for the coherent receiver.

Figure 3 shows the relation of the detector input SNR E_{LOS}/N_0 and the output LSNR based on (9) and (10). The specific curves for the energy detector (ED) are obtained by increasing ND by factors of four. The depicted curves correspond to $N_{pr} = [16, 64, 256, 1024, 4096]$, $N_s = 31$, $T_I = 2$ ns, and $W_{RRC} = 1$ GHz. Note that $N_{pr} = 256$ is not included in the standard. The curves are separated if the quadratic noise term dominates and they merge if the linear noise term is dominant. Increasing E_{LOS}/N_0 by 6 dB leads to LSNR +12 dB in the quadratic part and to +6 dB in the linear one. The horizontal line illustrates the LSNR at the working point $\text{LSNR}_{WP} = 12$ dB for the energy detector (cf. [16]). At this working point, 80% of the range estimates are within 1 m. The coherent receiver shows a working point $\text{LSNR}_{WP} = 9$ dB (cf. [21]). Both working points have been determined by extensive simulations (see [15]). It can be seen for the energy detector that 3 dB more E_{LOS}/N_0 are required when N_{pr}, the number of sequence repetitions, is increased by a factor of four. Note that the quadratic noise term dominates at this working point. As observable from (9), the LSNR for the coherent receiver is independent of the number of the pulses. It depends only on the transmitted energy. In other words, it does not matter if this energy is transmitted in one pulse or in a sequence of pulses. The coherent receiver shows an advantage ≥11 dB in the working point in comparison to the noncoherent receiver.

Table 2: Link budget.

Parameter		Values
Pulse energy (incl. G_{TX})	E_p	−116.38 dBWs
Preamble energy	E_{pr}	−74.31 dBWs
Free space loss at 1 meter	L_{fs}	−45.5 dB
Receiver antenna gain	G_{RX}	0 dBi
Received LOS component energy	$\widetilde{E}_{LOS}$	−119.81 dBWs
Noise spectral density	N_0	−198.93 dBW/Hz
Implementation loss	L_{imp}	4 dB
Fading margin	M_F	3 dB
Receiver input SNR	$E_{LOS}/N_0(1\,\text{m})$	72.12 dB

2.3. Maximal Operating Distance. As N_0 is constant in the scenario, E_{LOS}/N_0 for the maximal operating distance d_{max} is obtained from the well-known pathloss model

$$\frac{E_{LOS}}{N_0}(d_{max})_{dB} = \frac{E_{LOS}}{N_0}(d_0)_{dB} - 10\eta \log\left(\frac{d_{max}}{d_0}\right), \tag{11}$$

where η is the pathloss exponent and d_0 is a reference distance. The maximal operating distance for the coherent receiver is obtained from (9) and (11):

$$d_{max} = \left(\frac{(E_{LOS}/N_0)(1\,\text{m})}{(E_{LOS}/N_0)(d_{max})}\right)^{1/\eta} = \left(\frac{(E_{LOS}/N_0)(1\,\text{m})}{\text{LSNR}_{WP}}\right)^{1/\eta}, \tag{12}$$

where the reference distance d_0 is assumed to be 1 m. It follows for the energy detector

$$d_{max} = \left(\frac{(E_{LOS}/N_0)(1\,\text{m})}{\text{LSNR}_{WP} + \sqrt{\text{LSNR}_{WP}\,(\text{LSNR}_{WP} + \text{ND}/2)}}\right)^{1/\eta} \tag{13}$$

using (10) in (11).

2.4. Maximal Allowed Pathloss PL_{max}. A more general look at the achievable range is given by the maximal allowed pathloss, which is independent of the channel model, fading margins, or implementation losses. The pathloss model can be rewritten with (9) to obtain PL_{max} for the coherent receiver

$$\text{PL}_{max,dB} = \frac{\widetilde{E}_{LOS}}{N_0}(1\,\text{m})_{dB} - \text{LSNR}_{WP,dB}, \tag{14}$$

where $\widetilde{E}_{LOS}$ is the energy of the received LOS component at 1 m, which does not take fading margins or implementation losses into account (see Table 2).

For the energy detector follows, using (10) and (11),

$$\begin{aligned}\mathrm{PL}_{\max,\mathrm{dB}} &= \frac{\widetilde{E}_{\mathrm{LOS}}}{N_0}(1\,\mathrm{m})_{\mathrm{dB}} \\ &\quad - 10\log\left(\mathrm{LSNR}_{\mathrm{WP}} + \sqrt{\mathrm{LSNR}_{\mathrm{WP}}\left(\mathrm{LSNR}_{\mathrm{WP}} + \frac{\mathrm{ND}}{2}\right)}\right).\end{aligned} \tag{15}$$

$E_{\mathrm{LOS}}/N_0(1\,\mathrm{m})$ and $\widetilde{E}_{\mathrm{LOS}}/N_0(1\,\mathrm{m})$ are defined by the transmitted preamble energy E_{pr} (see Section 3) and the link budget (see Section 4).

3. FCC Regulations

In this section, the maximal allowed transmit power is calculated with respect to the FCC regulations [19]. In principle, the same regulations have been adopted by the CEPT in Europe for the band between 6 and 8.5 GHz [20]. In the band between 3.1 and 4.8 GHz, the CEPT requires detect and avoid (DAA) or low duty cycle (LDC) mitigation additionally, which does not influence this analysis. This analysis is done in accordance to [18].

The FCC constraints essentially consist of an average and a peak power limit. In any band of bandwidth $B_{\mathrm{av}} = 1\,\mathrm{MHz}$, the average transmit power is limited to $P_{\mathrm{av}}^{\mathrm{FCC}} = -41.3\,\mathrm{dBm}$ for an averaging window of $T_{\mathrm{av}} = 1\,\mathrm{ms}$. The peak power within the bandwidth $B_{\mathrm{pk}} = 50\,\mathrm{MHz}$ is restricted to $P_{\mathrm{pk}}^{\mathrm{FCC}} = 0$ dBm. Both peak and average transmit power are defined by the equivalent isotropically radiated power (EIRP).

The 802.15.4a preamble is a sequence of nonuniformly spaced pulses whose polarities are chosen pseudorandomly by the codes. According to [18], its average and peak power are determined by ERF and PRF, respectively. The pulse energy spectral density (ESD) $E_{p,\mathrm{av}}|W(f_c)|^2$ for the average power limit is given by

$$E_{p,\mathrm{av}}\left|W(f_c)\right|^2 = \begin{cases} \dfrac{T_{\mathrm{av}}P_{\mathrm{av}}^{\mathrm{FCC}}}{2B_{\mathrm{av}}}, & \mathrm{ERF} \le \dfrac{1}{T_{\mathrm{av}}}, \\ \dfrac{P_{\mathrm{av}}^{\mathrm{FCC}}}{2B_{\mathrm{av}}\mathrm{ERF}}, & \mathrm{ERF} \ge \dfrac{1}{T_{\mathrm{av}}}, \end{cases} \tag{16}$$

where $E_{p,\mathrm{av}}$ is the pulse energy limited by the average power limit and $W(f_c)$ is the spectrum of the normalized pulse $w(t)$ at the center frequency f_c. ERF is defined as

$$\mathrm{ERF} = \begin{cases} \mathrm{MRF}\dfrac{T_{\mathrm{pr}}}{T_{\mathrm{av}}} = \dfrac{M_1}{T_{\mathrm{av}}} & T_{\mathrm{pr}} < T_{\mathrm{av}} \\ \mathrm{MRF} & T_{\mathrm{pr}} \ge T_{\mathrm{av}} \end{cases} \tag{17}$$

where $M_1 = (N_s + 1)/2$ is the number of code elements not equal to zero. ERF is the compressed MRF due to stretching the preamble over the averaging time $T_{\mathrm{av}} = 1\,\mathrm{ms}$ (FCC). If T_{pr} is greater than T_{av}, then it is MRF. The mean power is limited by the number of pulses within 1 ms ($N_{1\,\mathrm{ms}}$) (see Table 1).

The peak power limit is defined by the PRF, where the sequenced pulses within an observation window $1/B_{\mathrm{pk}} = 20\,\mathrm{ns}$ are added. The ESD $E_{p,p}|W(f_c)|^2$ for the peak power limit is obtained by

$$E_{p,p}\left|W(f_c)\right|^2 = \begin{cases} \dfrac{P_{\mathrm{pk}}^{\mathrm{FCC}}}{9B_{\mathrm{pk}}^2}, & \mathrm{PRF} \le \left(\dfrac{3}{2}\right)B_{\mathrm{pk}}, \\ \dfrac{P_{\mathrm{pk}}^{\mathrm{FCC}}}{4\mathrm{PRF}^2}, & \mathrm{PRF} \ge \left(\dfrac{3}{2}\right)B_{\mathrm{pk}}, \end{cases} \tag{18}$$

where $E_{\mathrm{p,p}}$ is the pulse energy limited by the peak power limit.

The maximal FCC compliant pulse ESD with respect to peak and average power is shown in Figure 4. To find the active ESD for a specific preamble, the smaller value between $\mathrm{ESD}_{\mathrm{pk}}$ at PRF and $\mathrm{ESD}_{\mathrm{av}}$ at ERF is considered. The peak power limit for the short preamble symbols with $L = 16$ and $L = 64$ is the same, while, for the long preamble sequences it is lower due to higher PRF. It can be observed that only the preamble sequences with $N_{\mathrm{pr}} = 16$ are peak power limited. However, it is reported in [22] that the supply voltage limits the transmit power in low-data-rate systems and the peak power limit cannot be exploited for low supply voltages.

Assuming a pulse with rectangular spectrum, the energy per pulse $E_p = 2BE_p|W(f_c)|^2$, where B is the pulse bandwidth. Thus, the achievable preamble SNR can be calculated as shown in Figure 5. At $N_{\mathrm{pr}} = 16$, all preamble codes are limited by the peak power limit. The long preamble symbols contain approximately. 2 dB more energy in four times more pulses. Increasing the number of pulses does not necessarily lead to a preamble energy improvement, if $T_{\mathrm{pr}} \le 1\,\mathrm{ms}$, because the long preamble symbols and the short codes with spreading $L = 16$ are mean power limited between $N_{\mathrm{pr}} = 64$ and 1024. $N_{\mathrm{pr}} = 4096$ leads to an improvement, because $T_{\mathrm{pr}} > 4\,\mathrm{ms}$, which means the preamble is more than four times longer than T_{av}. The short preamble codes with spreading 64 imply a four times longer preamble in contrast to the others, thus a gain of up to 6 dB can be achieved.

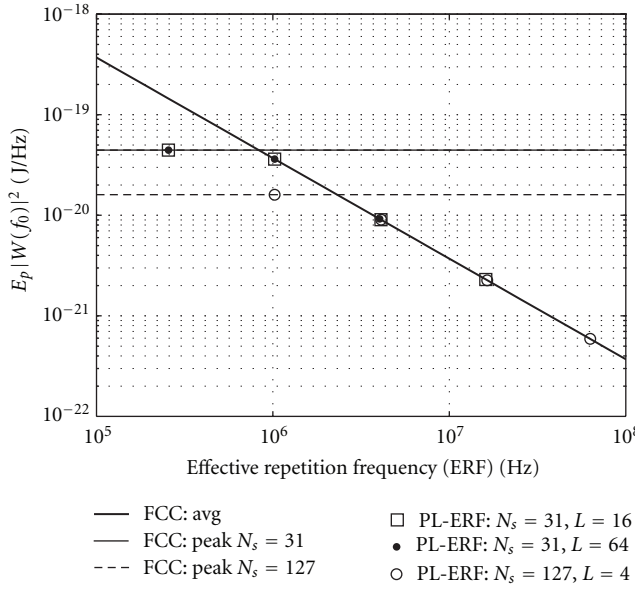

Figure 4: Pulse energy spectral density.

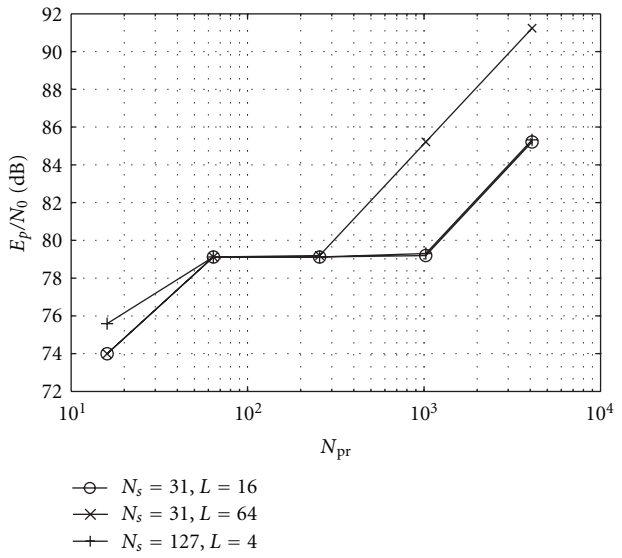

Figure 5: Achievable preamble energies.

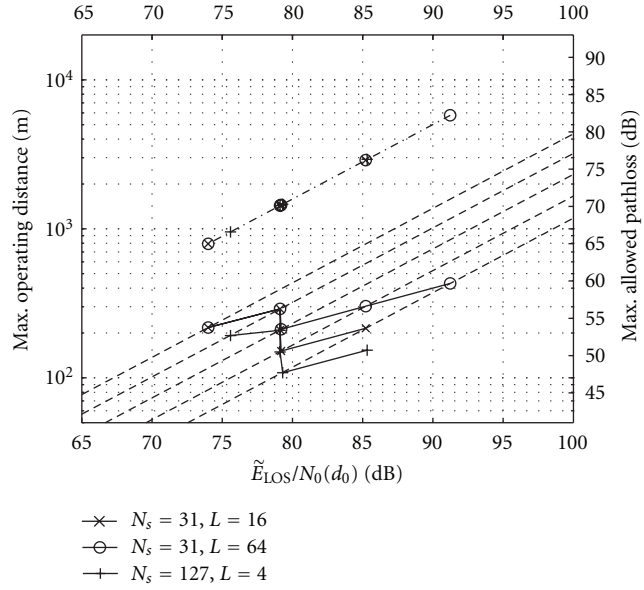

Figure 6: Code sequence analysis on the maximal operating distance and the maximal allowed pathloss, where the solid lines correspond to the energy detector, the dashed-dotted lines belong to the coherent receiver, and the dashed lines indicate constant noise dimensionality for the energy detector. The values are given for $N_{pr} = [16, 64, 256, 1024, 4096]$ (from left to right).

4. Link Budget

As mentioned before, $E_{LOS}/N_0(1\,\text{m})$ is the input SNR of the receiver at 1 m which depends on the link budget. Table 2 shows an example link budget calculation for 802.15.4a channel (ch) 3, using $N_{pr} = 1024$, $N_s = 31$, $L = 16$, $f_c = 4.4928$ GHz, and a bandwidth of 499.2 MHz. In that case, the average power limit of the FCC regulations applies and E_p is calculated from (16), where also the antenna gain is included. E_p is limited for 1006 sequences due to averaging over 1 ms (see Table 1). The preamble energy $E_{pr} = E_p M_1$, the free space loss L_{fs} at 1 m is given by 45.5 dB using Friis' equation [23], and the receiver antenna gain G_{RX} is defined by 0 dBi. These values yield the received preamble energy without multipath components, meaning the energy of the line of sight component $\widetilde{E}_{LOS}$ at 1 m. Assuming the input structure of the receiver is linear, the noise spectral density is given by $N_0 = kT_0F$ [23], where the Boltzmann constant $k = 1.38 \times 10^{-23}$ Joule/Kelvin [J/K], the temperature of the environment $T_0 = 293$ K, and the noise figure of the receiver input structure $F = 5$ dB (cf. [24]). Implementation losses of 4 dB and a LOS fading margin of 3 dB are assumed. Thus, $E_{LOS}/N_0(1\,\text{m})$ is obtained and can be used to calculate the maximal operating range according to (11) and (13).

5. Results

The maximal operating distance and the maximal acceptable pathloss are analyzed in this section. The maximal operating distance is based on the free-space link budget, because the LOS component is needed for accurate ranging. The maximal acceptable pathloss is shown as a more general value, which allows the implementer to analyze the effect of specific channel models, for example, NLOS scenarios, or specific system parameters, for example, lower noise figures.

5.1. Effect of Codes. Figure 6 shows the maximal operating distance d_{max} and the maximal allowed pathloss PL_{max} with respect to the length N_{pr} of the preamble sequences. The coherent receiver is directly proportional to E_p/N_0, which means that the operating distance is related to the preamble energy discussed in Figure 5. By contrast, the ED suffers from noncoherent combining losses, thus the noise dimensionality including the number of transmitted pulses is important for the final performance (see (13)). A change of E_p/N_0 without changing the noise dimensionality, for example, using a different noise figure or pulse energy, leads to a shift of the curves along the dashed lines, but the shape of the curves does not change. Thus, the general conclusions are still valid, while d_{max} and PL_{max} need to be recalculated according to the new link budget.

In the overall performance there is a big gap between the CR and the ED. The CR achieves a maximal operating distance up to several thousand meters and the ED achieves only several hundred meters. However, an operating distance of several hundred meters is usually sufficient for (low-complexity) indoor localization systems and sensor networks.

As expected from Section 3, the best performance is achieved by the short preamble with long spreading ($L = 64$) which has the highest transmitted energy. A maximal operating distance of approximately 6000 m ($PL_{max} \approx 82$ dB) is achieved by the CR, and ≈430 m ($PL_{max} \approx 60$ dB) is achieved by the ED. The CR reaches approximately half of that distance (≈3000 m; $PL_{max} \approx 76$ dB) for the other two codes. As mentioned before, the energy detector shows a more specific behavior, which is discussed in detail in the rest

of this paragraph. As observable, the increasing of N_{pr} does not necessarily lead to a better performance. A performance degradation is seen at around $\widetilde{E}_{\mathrm{LOS}}/N_0(d_0) \approx 79\,\mathrm{dB}$ for increasing numbers of transmitted pulses due to constant transmitted energy (cf. Figure 5). This effect also harms the performance of the long preamble codes ($N_s = 127$) significantly and leads to the lowest performance achieved. The performance of the short preamble sequences ($N_s = 31$) with spreading $L = 16$ and the long preamble sequences ($N_s = 127$) is best at $N_{\mathrm{pr}} = 64$, where a distance of $\approx 300\,\mathrm{m}$ ($\mathrm{PL}_{\max} \approx 56\,\mathrm{dB}$) and $\approx 200\,\mathrm{m}$ ($\mathrm{PL}_{\max} \approx 53\,\mathrm{dB}$) is reached, respectively. The preamble sequences with $L = 64$ show a local optimum for $N_{\mathrm{pr}} = 64$ with the same performance as the $L = 16$ sequence. This performance is also obtained for a much longer preamble with $N_{\mathrm{pr}} = 1024$ repetitions and slightly improved with $N_{\mathrm{pr}} = 4096$ at the cost of increased preamble energy (cf. Figure 5), much longer signals (see Table 1), and much higher processing effort. From these results, it seems inefficient for EDs to choose extremely long preambles with $N_{\mathrm{pr}} \geq 1024$.

The IEEE 802.15.4a standard also defines different channels with specific bandwidths and carrier frequencies. An analysis of the various channels is given in the next section.

5.2. Effect of Frequency Channels. The IEEE 802.15.4a standard defines 16 channels in three frequency bands, the subgigahertz band (<1 GHz), the low band (3.2–4.8 GHz), and the high band (5.9 – 10.3 GHz). The channel bandwidths B range from 499.2 to 1354.97 MHz. As mentioned in Section 3, keep in mind that the CEPT allows only the usage of the frequency bands 3.1–4.8 and 6–8.5 GHz for UWB, where, for LDC, the signals have to be shorter than 5 ms. Thus, the short preamble symbol with spreading $L = 64$ and $N_{\mathrm{pr}} = 4096$ is not allowed for LDC transmission. It is well known that a higher carrier frequency f_c causes higher losses and thus less received signal strength according to Friis' equation. A larger bandwidth leads to a higher allowed transmit power (see Section 3). To evaluate this tradeoff, six channels are analyzed in this paper, using the short preamble codes with $L = 64$.

Figure 7 shows the relation between input and output SNR for the specific channels. As seen from (9), the CR is again independent of the channel bandwidths. For the ED, variations occur due to the different pulse and receiver bandwidths. It can be observed that the channels with the large bandwidths need up to 1.5 dB more E_p/N_0 in the working point to achieve the same LSNR.

Figure 8 shows the allowed preamble energies for the specific channels. The larger bandwidths of the preambles allow a gain of up to 4 dB, which is sufficient to compensate the SNR loss of the ED shown in Figure 7. This is also seen from (10), where the equivalent bandwidth W_{RRC} influences LSNR linearly and the additional energy improves the SNR quadratically in the working point. Thus, a gain of up to 2.5 dB can be achieved. For the CR, the additional energy will directly improve the performance.

Figure 9 shows the maximal operating distance and the maximal allowed pathloss for the specific channels. It can

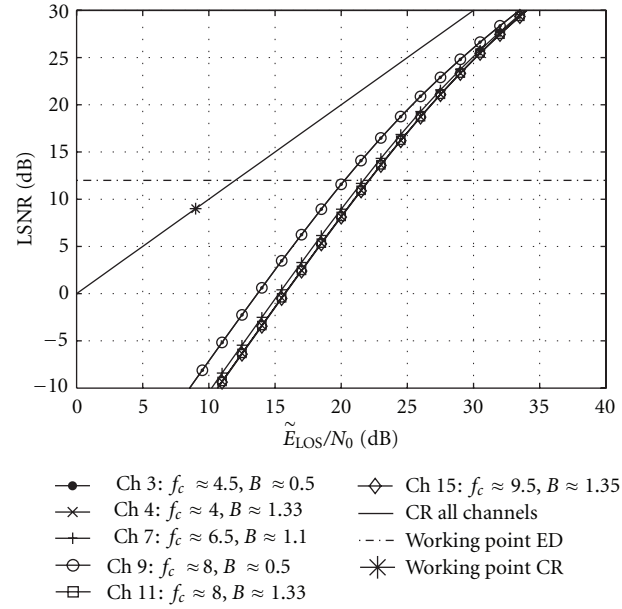

Figure 7: Relation between input SNR $\widetilde{E}_{\mathrm{LOS}}/N_0$ and output SNR LSNR for the short preamble codes with a spreading $L = 64$ and $N_{\mathrm{pr}} = 16$ with respect to the IEEE 802.15.4a channels. The channel parameters in the legend are in GHz.

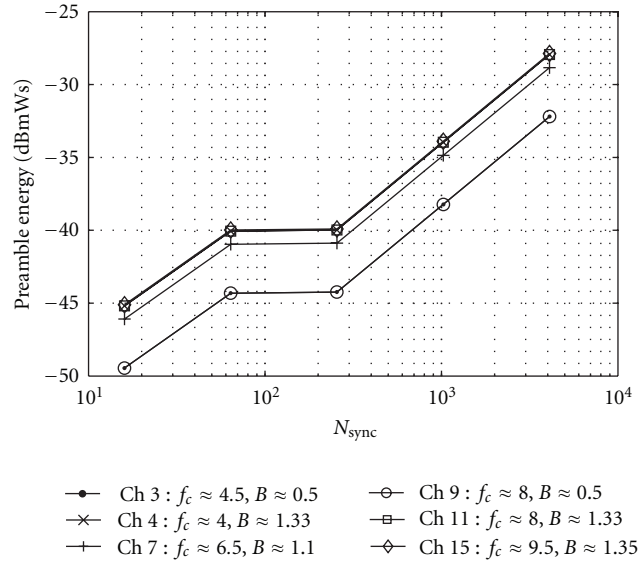

Figure 8: Allowed preamble energy for the specific IEEE802.15.4a channels.

be observed that the low-band channels (Ch 3 and Ch 4) perform better than the high-band channels due to lower free-space losses. Only half the operating range is obtained when f_c is increased from 4 to 8 GHz. A shift in the carrier frequency leads to a change of E_{LOS}/N_0, but it does not change the relation of input and output SNR (compare Ch 3 and Ch 9). A shift of the bandwidth changes this relation due to a change of ND, which is observable for Ch 9 and Ch 11. The operating range is doubled with the CR when the bandwidth is increased from 500 MHz to 1.33 GHz, while only the 1.3

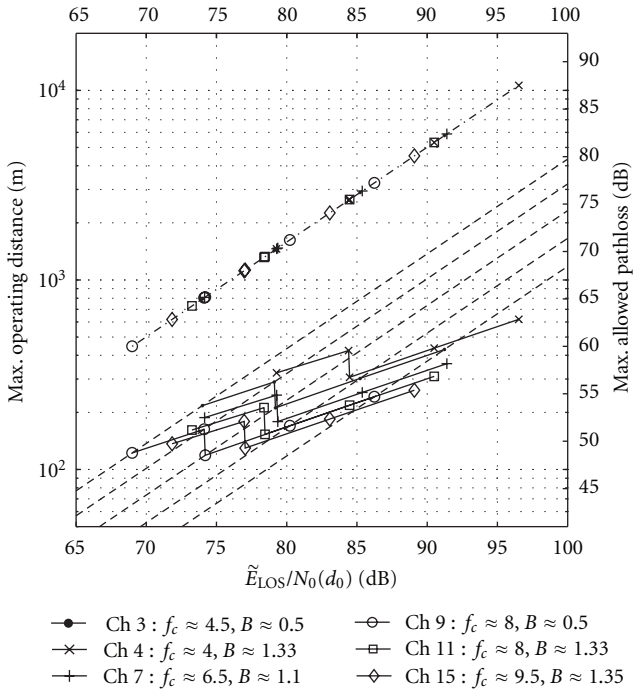

Figure 9: Maximal operating distance and maximal allowed pathloss for the specific IEEE 802.15.4a channels. The dashed lines show the characteristic for a channel with $B = 499.2$ MHz with the ND of Figure 6.

fold distance is achieved with the ED. The best performance is obtained at Ch 4, which has a low carrier frequency $f_c \approx 4$ GHz and a large bandwidth of $B \approx 1.33$ GHz. It reaches a $d_{\max} \approx 10620$ m ($\mathrm{PL}_{\max} \approx 88$ dB) for the CR and $d_{\max} \approx 620$ m for the ED ($\mathrm{PL}_{\max} \approx 63$ dB). The mandatory Ch 3 of the low band shows a significantly better performance in comparison to the mandatory channel in the high band Ch 9 due to the lower f_c.

6. Conclusions

A coherent receiver and an energy detector have been studied for ranging in IEEE 802.15.4a, in the sense of maximal allowed transmit energy, maximal operating distance, and maximum allowed pathloss.

The maximal allowed transmit energy according to the FCC/CEPT regulations depends strongly on the parameters of the preamble. For most of the preamble code sequences, the average power limit applies. A longer spreading of the preamble symbols leads to a performance gain, because a larger preamble energy is obtained. As the FCC/CEPT limits the power spectral density, a higher bandwidth leads to an increased energy too.

The maximal operating distance is calculated from the link budget. The coherent receiver directly depends on the receiver input SNR, while the energy detector is also influenced strongly by the parameters of the preamble codes due to the noncoherent combining loss. A 64-symbol repetitions preamble is most efficient for the energy detector due to lower noncoherent combining losses and the short preamble symbols are preferable due to less despreading effort. The channels from the low-frequency band achieve longer ranges due to the lower pathloss. The mandatory low-frequency channel ($f_c = 4.5$ GHz) achieves almost twice the range in comparison to the mandatory high-frequency channel ($f_c = 8$ GHz). A gain is obtained for the high-bandwidth channels. The range is almost doubled with the coherent receiver, while the energy detector reaches only a gain of 30 percent.

The low-complexity energy detector achieves maximal operating distances of several hundred meters, while the coherent receiver reaches distances up to several thousand meters in free-space. Thus, both receiver architecture are appropriate for real-time locating systems and sensor networks in typical indoor scenarios.

Acknowledgments

The authors would like to warmly thank G. Kubin, TU Graz, and M. Pistauer, CISC Semiconductor GmbH, for their support in the project. The project was funded by the Federal Ministry for Transport, Innovation and Technology (BMVIT) and the Austrian Research Promotion Agency (FFG).

References

[1] D. Harmer, M. Russell, E. Frazer et al., "EUROPCOM: emergency ultrawideband radio for positioning and Communications," in *Proceedings of the IEEE International Conference on Ultra-Wideband (ICUWB '08)*, pp. 85–88, 2008.

[2] J. Rantakokko, P. Hndel, and M. Fredholm, "User requirements for localization and tracking technology," in *Proceedings of the International Conference on Indoor Positioning and Indoor Navigation (IPIN '10)*, pp. 221–222, September 2010.

[3] M. Z. Win and R. A. Scholtz, "Impulse radio: how it works," *IEEE Communications Letters*, vol. 2, no. 2, pp. 36–38, 1998.

[4] Y. Qi and H. Kobayashi, "On relation among time delay and signalstrength based geolocation methods," in *Proceedings of the IEEE Global Telecommunications Conference (GLOBECOM '03)*, pp. 4079–4083, December 2003.

[5] L. Yang and G. B. Giannakis, "Ultra-wideband communications," *IEEE Signal Processing Magazine*, vol. 21, no. 6, pp. 26–54, 2004.

[6] S. Gezici, Z. Tian, G. B. Giannakis et al., "Localization via ultra-wideband radios: a look at positioning aspects of future sensor networks," *IEEE Signal Processing Magazine*, vol. 22, no. 4, pp. 70–84, 2005.

[7] I. Guvenc and Z. Sahinoglu, "Threshold-based TOA estimation for impulse radio UWB systems," in *Proceedings of the IEEE International Conference on Ultra-Wideband (ICU '05)*, pp. 420–425, che, September 2005.

[8] M. Z. Win, D. Dardari, A. F. Molisch, W. Wiesbeck, and J. Zhang, "History and applications of UWB," *Proceedings of the IEEE*, vol. 97, no. 2, pp. 198–204, 2009.

[9] N. A. Alsindi, B. Alavi, and K. Pahlavan, "Measurement and modeling of ultrawideband TOA-based ranging in indoor multipath environments," *IEEE Transactions on Vehicular Technology*, vol. 58, no. 3, pp. 1046–1058, 2009.

[10] IEEE Std., *Part 15.4: Wireless Medium Access Control (MAC) and Physical Layer (PHY) Specifications for Low-Rate Wireless*

Personal Area Networks(WPANs), Amendment 1: Add Alternate PHYs, 2007.

[11] Y. S. Kwok, F. Chin, and X. Peng, "Ranging mechanism, preamble generation, and performance with IEEE 802.15.4a low-rate low-power UWB systems," in *Proceedings of the IEEE 9th International Symposium on Spread Spectrum Symposium on Spread Spectrum Techniques and Applications (ISSSTA '06)*, pp. 430–434, bra, August 2006.

[12] M. Weisenhorn and W. Hirt, "Robust noncoherent receiver exploitingUWB channel properties," in *Proceedings of the International Workshop on Ultra Wideband Systems Joint with Conference on Ultrawideband Systems and Technologies (Joint UWBSTIWUWBS '04)*, pp. 156–160, 2004.

[13] K. Witrisal, G. Leus, G. J. M. Janssen et al., "Noncoherent ultra-wideband systems: An overview of recent research activities," *IEEE Signal Processing Magazine*, vol. 26, no. 4, pp. 48–66, 2009.

[14] A. A. D'Amico, U. Mengali, and L. Taponecco, "TOA estimation with the IEEE 802.15.4a standard," *IEEE Transactions on Wireless Communications*, vol. 9, no. 7, pp. 2238–2247, 2010.

[15] T. Gigl, *Low-complexity localization using standard-compliant UWB signals*, Ph.D. thesis, Graz University of Technology, Graz, Austria, 2010.

[16] T. Gigl, J. Preishuber-Pfluegl, and K. Witrisal, "Statistical analysis of a UWB energy detector for ranging in IEEE 802.15.4a," in *Proceedings of the IEEE International Conference on Ultra-Wideband (ICUWB '09)*, pp. 129–134, September 2009.

[17] B. Geiger, T. Gigl, J. Preishuber-Pfluegl, and K. Witrisal, "Experimental characterization of system parameters for ranging in IEEE 802.15.4a using energy detectors," *Radioengineering*, vol. 18, no. 3, pp. 249–257, 2009.

[18] F. Troesch, *Novel low duty cycle schemes: from ultra wide bandto ultra low power*, Ph.D. thesis, ETH Zurich, 2010.

[19] FCC, "Revision of part 15 of the commission's rules regarding ultra-widebandtransmission systems," First Report and Order, ET-Docket 98-153, FCC 02-28 Std., FCC, 2002.

[20] EC, "Commission Decision of 21 April 2009: amending Decision2007/131/EC on allowing the use of the radio spectrum for equipmentusing ultra-wideband technology in a harmonised manner in thecommunity," Official Journal of the European Union L105/9 Std., April 2009.

[21] T. Gigl, J. Preishuber-Pfluegl, D. Arnitz, and K. Witrisal, "Experimental characterization of ranging in IEEE802.15.4a using a coherent reference receiver," in *Proceedings of the IEEE 20th International Symposium in Personal, Indoor and Mobile Radio Communications*, pp. 92–96, September 2009.

[22] G. Kolumbán, T. Krébesz, C. K. Tse, and F. C.M. Lau, "Derivation of circuit specification for the UWB impulse radio transceivers," in *Proceedings of the IEEE International Symposium on Circuits and Systems: Nano-Bio Circuit Fabrics and Systems (ISCAS '10)*, pp. 337–340, 2010.

[23] L. Couch, *Digital and Analog Communication Systems*, Prentice Hall, Upper Saddle River, NJ, USA, 7th edition, 2007.

[24] G. Fischer, O. Klymenko, and D. Martynenko, "Time-of-arrival measurement extension to a non-coherent impulse radio UWB transceiver," in *Proceedings of the 5th Workshop on Positioning, Navigation and Communication (WPNC '08)*, pp. 265–270, March 2008.